17th World Conference on Earthquake Engineering, 17WCEE
Sendai, Japan - September 13th to 18th 2020

Semi-active control of base-isolated structure using MR damper that simulates variable hydraulic damper and complex stiffness damper

A. Kishida[1], E. Sato[2], S. Iba[3], H. Fujitani[4], Y. Mukai[5], K. Itahara[3] , E. Johnson[6], K. Kajiwara[7]

[1] *Research Fellow, National Research Institute for Earth Science and Disaster Resilience, akiko_kishida@bosai.go.jp*
[2] *Chief Researcher, National Research Institute for Earth Science and Disaster Resilience, eiji@bosai.go.jp*
[3] *Graduate Student, Kobe University*
[4] *Professor, Kobe University, fujitani@kobe-u.ac.jp*
[5] *Associate Professor, Kobe University, ymukai@port.kobe-u.ac.jp*
[6] *Professor, Department of Civil and Environmental Engineering, University of Southern California, johnsone@usc.edu*
[7] *Principal Chief Researcher, National Research Institute for Earth Science and Disaster Resilience, kaji@bosai.go.jp*

Abstract

Semi-active control strategies were devised to decrease both deformation and acceleration response of a base-isolation system under near-fault pulsed ground motions. The authors employed two control strategies in the shaking table tests of E-Defense using a large-scale base-isolated building model and a magnetorheological (MR) damper: (1) control system that simulates a semi-active hydraulic damper and (2) control system that simulates a complex stiffness damper.

(1) The semi-active hydraulic damper was designed to switch the damping coefficient between two phases. The authors set two damping coefficients equivalent to 10% and 30% damping factors, or c_{L} and c_{H}, respectively. The ideal control force was calculated using LQ theory. In one method, the damping coefficient is set to be c_{H} when the output force of the damper becomes smaller than the ideal control force, or the damping coefficient is set to be c_{L} when the output force becomes greater than or equal to the ideal control force; however, this method causes chattering. To prevent the chattering, we adopted the original strategy in which the damping coefficient stays at c_{L} while the velocity direction is the same; once the output force of the damper becomes greater than or equal to the ideal control force, the damping coefficient is switched to c_{L}. Passive control tests in which the damping coefficients of the passive damper were c_{L} and c_{H} were also conducted. Our proposed control system demonstrated a performance that was almost equal to the passive control system for the isolation deformation; furthermore, it can restrain the increase of the floor acceleration caused by a larger damping coefficient.

(2) Complex damping is well known as an effective damping mechanism for a base-isolation system. The authors reproduced the damping force of a complex stiffness damper with an MR damper. The damping force of the complex stiffness damper was determined from the relative story displacement at the time after 1/4 of the natural period of the structure. To simulate the damping force, the authors designed two digital filters, a Butterworth filter and a phase-delay-compensation filter. The order of the Butterworth filter was set to 1 and the cut-off frequency was set to 0.043. The phase-delay-compensation filter was designed to reduce the phase lag at the natural frequency of the structure. By applying these two digital filters to the relative velocity of the superstructure and multiplying this by the damping coefficient, the ideal control force was calculated. The damping force was reduced in comparison with the passive viscous damping for the response to El Centro, Sylmar, and Takatori waves, although the response reduction effect was almost equal to the passive viscous damping.

Furthermore, real-time hybrid simulations using the same MR damper were conducted, and our proposed control strategies revealed the effectiveness for the ideal base-isolated structure models.

Keywords: Semi-active hydraulic damper, Complex stiffness damper, Shaking table test, Real-time hybrid simulation

1. Introduction

Seismic isolation systems are increasingly being used in Japan to minimize damage to building structures during earthquakes, such as the 1995 Hyogo-ken Nanbu earthquake. Large-magnitude earthquakes focused offshore or occurring directly above their foci, including long-period and long-duration earthquakes, can cause excessive deformation in the base-isolation layer. Furthermore, hardening the isolation device causes an increased response to acceleration, and it becomes difficult to maintain the safety and performance of the base-isolation system. Semi-active control using variable damping devices, such as magnetorheological (MR) dampers, is one of the available methods to prevent an increased response [1-3]. This paper proposes two control strategies for a semi-active control that simulates a semi-active hydraulic damper and a complex stiffness damper. The proposed control method that simulates a semi-active hydraulic damper is designed with control by a linear–quadratic regulator (LQR) and contrived not to induce chattering. Kumagai et al. confirmed that the damping force of the complex stiffness damper depends on only the response displacement, and the complex stiffness damper needs less control force than the passive viscous damper to obtain the same effect of displacement reduction [4]. We designed two digital filters to simulate the complex stiffness damper. A shaking table test using a large-scale base-isolated building model and an MR damper was conducted at the E-Defense center to verify our proposed control strategies. The semi-active hydraulic damper can reduce the absolute acceleration response, and the complex stiffness damper can reduce the damping force compared with a passive viscous damper.

2. Control system that simulates semi-active hydraulic damper

2.1 Control strategy

The semi-active hydraulic damper can switch the damping coefficient between two phases. The mass of the test specimen is 14.9 tons, and the stiffness of the isolation layer is 38.5 kN/m. We set two damping coefficients equivalent to 10% and 30% damping factors, $c_{\mathrm{L}} = 4.79\,\mathrm{kN\cdot s/m}$ and $c_{\mathrm{H}} = 14.37\,\mathrm{kN\cdot s/m}$. During one-directional shaking, the coordinate axis is assumed to be positive on the right. The following notation is used: F_i is the damping force on the *i*-th step, with the left side being positive; Ft_i is the ideal control force on the *i*-th step, with the left side being positive; d_i is the relative story displacement of the isolation layer on the *i*-th step; v_i is the relative velocity of the isolation layer on the *i*-th step; cd_i is the condition of the semi-active hydraulic damper on the *i*-th step; and c_i is the controlled damping coefficient on the *i*-th step.

The ideal control force was calculated according to LQ theory. In one method, the damping coefficient is set to c_{H} when the output force of the damper becomes smaller than the ideal control force, and the coefficient is set to c_{L} when the output force becomes greater than or equal to the ideal control force; however, this method causes chattering and the response acceleration increases. To prevent the chattering, we adopted the original strategy that the damping coefficient stays at c_{L} while the velocity direction is the same, and once the output force of the damper becomes greater than or equal to the ideal control force, the damping coefficient is switched to c_{L}. The strategy is as follows:

① When $v_i > 0$ ($F_i > 0$)

IF ($F_i < Ft_i \cap cd_{(i-1)} \neq 1$)

$cd_i = 2$

ELSE IF ($F_i \geq Ft_i \cup cd_{(i-1)} = 1$)

$cd_i = 1$

ELSE $cd_i = 3$

END (1)

② When $v_i < 0$ ($F_i < 0$)

IF ($F_i > Ft_i \cap cd_{(i-1)} \neq -1$)
$cd_i = -2$
ELSE IF ($F_i \leq Ft_i \cup cd_{(i-1)} = -1$)
$cd_i = -1$
ELSE $cd_i = -3$
END (2)

③ When $v_i = 0$ ($F_i = 0$)

$cd_i = 0$. (3)

The damping coefficient at the (i+1)-th step c_{i+1} changes as follows, depending on the value of cd_i :

IF ($cd_i = 1 \cup cd_i = -1$)
$c_{i+1} = c_L$
ELSE IF ($cd_i = 2 \cup cd_i = -2$)
$c_{i+1} = c_H$
ELSE $c_{i+1} = c_L$
END (4)

2.2 Shaking table test

The E-Defense shaking table test was conducted using the base-isolated testbed and an MR damper controlled by the strategy presented in subsection 2.1. The test specifications and input waves were as shown in [5]. The ideal LQ control force was calculated by $Ft_i = \alpha d_i + \beta v_i$. From the previous parametric studies, the first parameters were set to be $\alpha = -33.46$ and $\beta = 12.56$ (NIED1). In the middle of the experiment, it was found that the stiffness of the isolation layer was larger than the assumption, and an unexpected friction force was acting on the isolation layer. Then parametric studies with assumptions that the stiffness was 49.5 kN/m and the friction force was 3 kN were conducted, and a second set of parameters was set to be $\alpha = -40.84$ and $\beta = 15.19$ (NIED2). In the previous parametric studies, the damping factor of the structure was set to be 1%.

Fig. 1(a) shows the time history waveforms of the relative story displacement for the isolation layer for both NIED1 and NIED2 controlled dampers and two passive viscous damping factors of 10% and 30% when an El Centro wave is input. Fig. 1(b) shows the time history waveforms of the absolute acceleration for the top floor of the test specimen for the NIED1 controlled damper and passive viscous damping of 10% when an El Centro wave is input. Further, Fig. 1(c) shows the NIED1 controlled damper and passive viscous damping of 30%, Fig. 1(d) shows the NIED2 controlled damper and passive viscous damping of 10%, and Fig. 1(e) shows the NIED2 controlled damper and passive viscous damping of 30% when an El Centro wave is input. Fig. 2(a)–(e) shows the corresponding time history waveforms when a Takatori wave is input, and Fig. 3(a)–(e) shows the waveforms when a Sylmar wave is input.

Table 1 shows the maximum values of the relative story displacements for the isolation layer and the absolute accelerations for the top floor of the test specimen for the NIED1 and NIED2 controlled dampers and passive viscous damping of 10% and 30% when El Centro, Takatori, and Sylmar waves are input. Hereafter, NIED1 and NIED2 controlled dampers are noted as NIED1 and NIED2, and passive viscous dampers with 10% and 30% damping factors are referred to as 10% and 30%, respectively.

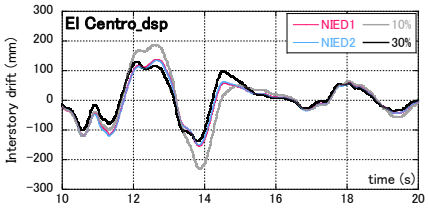

Fig. 1(a) – Relative story displacement (El Centro)

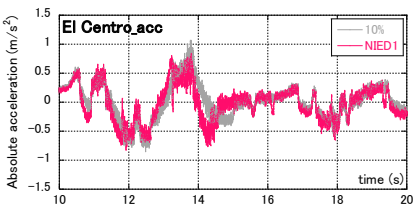

Fig. 1(b) – Absolute acceleration (El Centro, NIED1 vs. 10%)

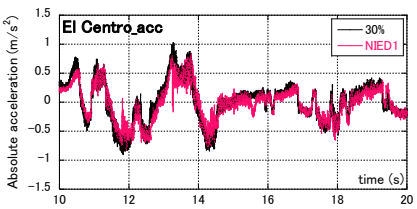

Fig. 1(c) – Absolute acceleration (El Centro, NIED1 vs. 30%)

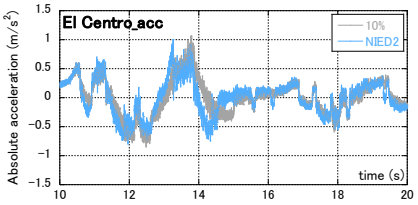

Fig. 1(d) – Absolute acceleration (El Centro, NIED2 vs. 10%)

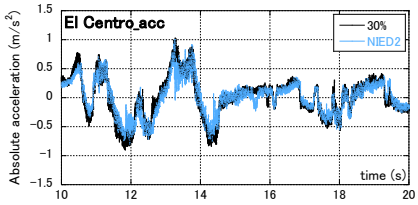

Fig. 1(e) – Absolute acceleration (El Centro, NIED2 vs. 30%)

Fig. 1 – Time history waveforms of relative story displacement for isolation layer and absolute acceleration for top floor of the test specimen when El Centro wave is input

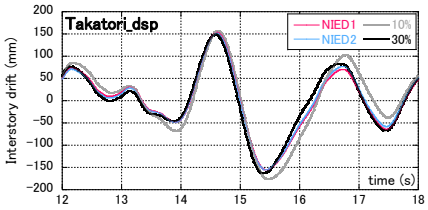

Fig. 2(a) – Relative story displacement (Takatori)

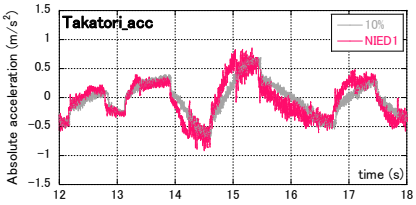

Fig. 2(b) – Absolute acceleration (Takatori, NIED1 vs. 10%)

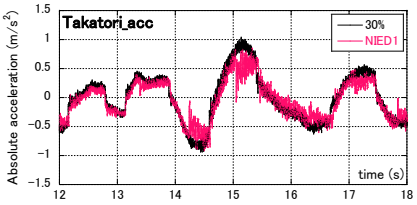

Fig. 2(c) – Absolute acceleration (Takatori, NIED1 vs. 30%)

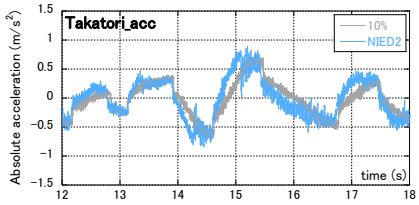

Fig. 2(d) – Absolute acceleration (Takatori, NIED2 vs. 10%)

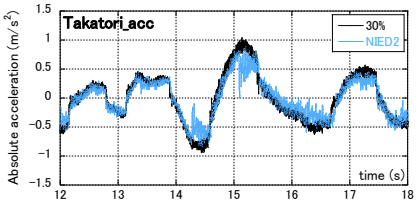

Fig. 2(e) – Absolute acceleration (Takatori, NIED2 vs. 30%)

Fig. 2 – Time history waveforms of relative story displacement for isolation layer and absolute acceleration for top floor of the test specimen when Takatori wave is input

The maximum values of relative story displacement for NIED1 and 2 are between those for 10% and 30% when El Centro and Sylmar waves are input, as expected. When a Takatori wave is input, the values are unexpectedly smaller than those for 10% and 30%. The maximum values of absolute acceleration for both NIED1 and 2 are between those for 10% and 30% when Takatori and Sylmar waves are input. When an El Centro wave is input, the values are smaller than those for 10% and 30%, especially in the case of NIED1, which is about 0.8 times as large as those for 10% and 30%.

As shown in Fig. 1(b),(c), immediately before each acceleration for 10% and 30% becomes the maximum, the damping coefficient changes and the acceleration increase is restrained. In Fig. 2(c),(e) and Fig. 3(c),(e),

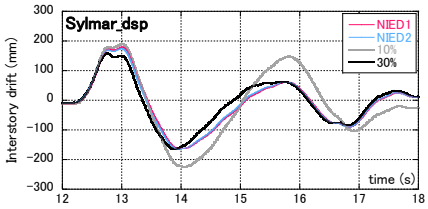

Fig. 3(a) – Relative story displacement (Sylmar)

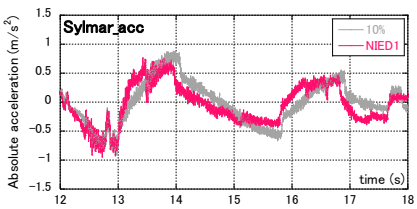

Fig. 3(b) – Absolute acceleration (Sylmar, NIED1 vs. 10%)

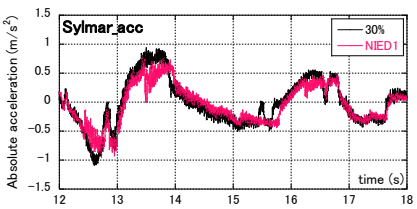

Fig. 3(c) – Absolute acceleration (Sylmar, NIED1 vs. 30%)

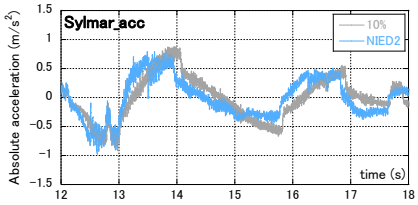

Fig. 3(d) – Absolute acceleration (Sylmar, NIED2 vs. 10%)

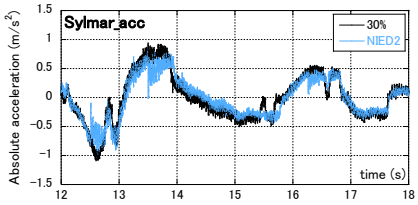

Fig. 3(e) – Absolute acceleration (Sylmar, NIED2 vs. 30%)

Fig. 3 – Time history waveforms of relative story displacement for isolation layer and absolute acceleration for top floor of the test specimen when Sylmar wave is input

Table 1 – Maximum values of relative story displacement and absolute acceleration for all input waves and control strategies (E-Defense experiment)

Control	Interstory drift (mm)			Absolute acceleration (m/s^2)		
	El Centro	Takatori	Sylmar	El Centro	Takatori	Sylmar
NIED1	154.0	155.4	179.3	0.84	0.91	0.94
NIED2	150.3	155.4	174.6	1.00	0.89	0.97
10%	230.2	176.7	224.3	1.06	0.70	0.91
30%	138.1	163.8	164.5	1.03	1.04	1.09

it is observed that the damping coefficient of 30% changes to 10% before the acceleration becomes the maximum. For all input earthquake waves, the maximum accelerations of NIED1 and NIED2 are less than those of 30%, showing that the proposed control method can restrain an increase of the acceleration because of a larger damping coefficient.

2.3 Real-time hybrid simulation

First, a real-time hybrid simulation (RTHS) with the same MR damper used in the E-Defense test was conducted. When the stiffness of the isolation layer was set to be 42.3 kN/m, the friction force of the isolation layer was 2 kN, and the damping coefficient of the isolation layer was 1.80 kN s/m or 2.90 kN s/m, and the results of RTHS almost agreed with those of the E-Defense test. Second, an RTHS with the same characteristics of the system tested previously was conducted with the following assumed conditions of the isolation layer: the stiffness of the isolation layer was 38.5 kN/m, the friction force of the isolation layer was 0 kN, and the damping coefficient of the isolation layer was 0.48 kN s/m (1% damping factor). The test results are discussed below.

Fig. 4(a) and Fig. 4(b) show the time history waveforms of the relative story displacement for the isolation layer and the absolute acceleration for the top floor of the test specimen, respectively, for NIED1, 10%, and 30% when an El Centro wave is input to the RHTS. Fig. 5(a) and Fig. 5(b) show the corresponding time

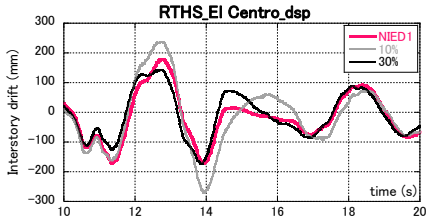

Fig. 4(a) – Relative story displacement (El Centro, RTHS)

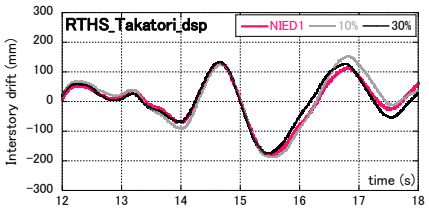

Fig. 5(a) – Relative story displacement (Takatori, RTHS)

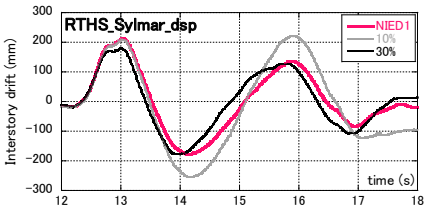

Fig. 6(a) – Relative story displacement (Sylmar, RTHS)

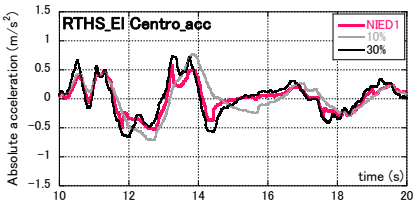

Fig. 4(b) – Absolute acceleration (El Centro, RTHS)

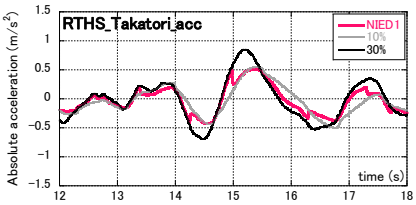

Fig. 5(b) – Absolute acceleration (Takatori, RTHS)

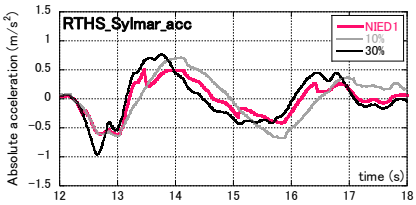

Fig. 6(b) – Absolute acceleration (Sylmar, RTHS)

Table 2 – Maximum values of interstory drifts and absolute accelerations for all input waves and control strategies (RTHS).

Control	Interstory drift (mm)			Absolute acceleration (m/s^2)		
	El Centro	Takatori	Sylmar	El Centro	Takatori	Sylmar
NIED1	180.1	179.4	213.7	0.58	0.52	0.61
10%	269.4	215.4	255.6	0.76	0.61	0.71
30%	172.8	175.7	179.6	0.74	0.85	0.96

history waveforms when a Takatori wave is input, and Fig. 6(a) and Fig. 6(b) show the waveforms when a Sylmar wave is input. Table 2 shows the maximum values of the relative story displacements for the isolation layer and the absolute accelerations for the top floor of the test specimen, for NIED1, 10%, and 30%, when El Centro, Takatori, and Sylmar waves are input to the RTHS.

The maximum values of relative story displacement for NIED1 are between those for 10% and 30% for all input waves, as expected. The maximum values of absolute acceleration for NIED1 are smaller than those for 10% and 30% for all input waves. As shown in Fig. 4(b), Fig. 5(b), and Fig. 6(b), the damping coefficient changes before the accelerations controlled by 10% and 30% reach their peaks, which restrains the acceleration increase. Under ideal conditions of the isolation layer, the response accelerations can be effectively reduced by our proposed control strategy.

3. Control system that simulates complex stiffness damper

3.1 Control strategy

This section discusses the control strategy that simulates the complex stiffness damper using an MR damper.

3.1.1 Complex stiffness damper

Eq. (5) is the equation of motion for the single-degree-of-freedom (SDOF) system that represents a base-isolated building whose isolation layer has a complex stiffness damper, and Eq. (6) determines the damping force.

$$m\ddot{x} + (k + 2\beta ki)x = -m\ddot{x}_g, \quad (5)$$

$$f_c(t) = 2\beta kix(t) = 2\beta kiX e^{i\omega t}, \quad (6)$$

where m is the lumped mass, k is the stiffness, x is the response displacement, x_g is the ground displacement, β is the complex damping factor, f_c is the damping force of the complex stiffness damper, and i is the imaginary unit.

It is obvious from Eq. (6) that the complex stiffness damper does not depend on the frequency; rather, it outputs a force value proportional to the displacement amplitude. The multiplication by imaginary unit i in Eq. (6) means that the damping force is allowed to advance by $\pi/2$ with respect to the response displacement in the frequency domain. It is impossible to obtain the displacement 1/4 of the natural period later (the phase is allowed to be advanced by $\pi/2$) from only information until the present time, and the complex stiffness damper does not have a causal relation in the time domain.

3.1.2 Relationship between control force of complex stiffness damper and passive viscous damper

As shown in Eq. (5), the damping force of the complex stiffness damper f_c can be obtained from that of the passive viscous damper f_v.

$$f_c = (\omega_0/\omega)f_v, \quad (7)$$

where f_v is the damping force of the passive viscous damper, ω is the natural circular frequency of ground motion, and ω_0 is the the natural circular frequency of the lumped mass system.

The transformation of Eq. (7) is the target transformation, and the digital filter is used to simulate it.

3.1.3 Design of digital filter

To simulate the target transformation, a Butterworth filter (1 degree and block frequency of 0 Hz), whose passable range is flat, was adopted. Fig. 7 shows the frequency properties of this Butterworth filter and the target filter. As Fig. 7 shows, the frequency property of the target transformation is closely simulated by the Butterworth filter. However, the phase property is late by 90 degrees after passing through the Butterworth filter, and there is a difference from the flat phase property of the target filter. To compensate for the phase delay, we designed a compensation filter to advance the phase. Fig. 8 shows the frequency properties of this compensation filter for phase advance and the target filter. As shown in Fig. 8, the compensation filter for phase advance can cancel the phase delay.

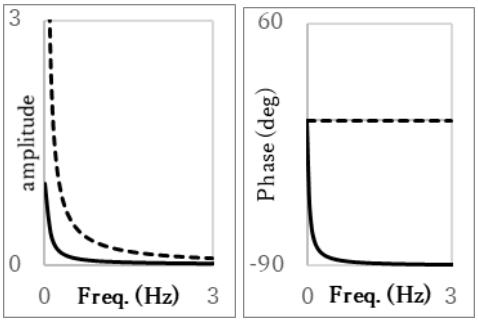

Fig. 7 – Frequency properties of Butterworth filter

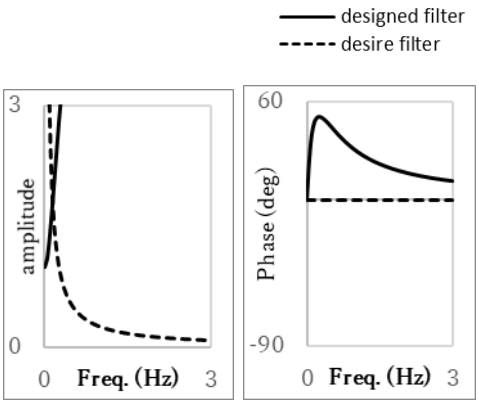

Fig. 8 – Frequency properties of compensation filter

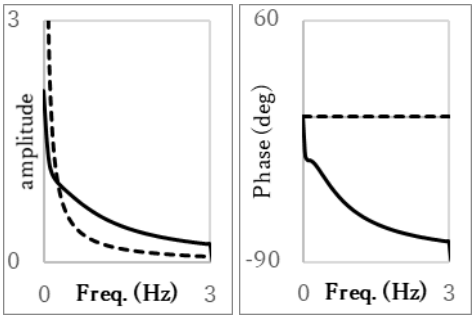

Fig. 9 – Frequency properties of designed filter

Table 3 – Parameters for design of filters.

Cutoff frequency (Hz)	0.043
Degrees	2.0

The target transformation was simulated by arranging the Butterworth filter and the compensation filter for phase advance in parallel. To avoid changing the amplitude property because of the compensation filter for phase advance, the parameters needed for the design of each filter were set as in Table 3. Fig. 9 shows the frequency properties of this filter and the target filter.

3.1.4 Simulation of complex stiffness damper using MR damper

The complex stiffness control using the designed filters was compared with the behavior of the target complex stiffness damper. The control force and the response displacement of the target damper are calculated from the transfer functions of Eqs. (8) and (9) and the input earthquake acceleration.

$$H_X^C(i\omega) = -\frac{1}{-\omega^2 + 2\beta{\omega_0}^2\mathrm{sgn}(\omega)i + {\omega_0}^2}, \tag{8}$$

$$H_F^C(i\omega) = -\frac{(2\beta{\omega_0}^2\mathrm{sgn}(\omega)i)m}{-\omega^2 + 2\beta{\omega_0}^2\mathrm{sgn}(\omega)i + {\omega_0}^2}, \tag{9}$$

where $H_X^C(i\omega)$ is the transfer function of the response displacement for the lumped mass system that possesses the complex stiffness damper and $H_F^C(i\omega)$ is the transfer function of the damping force of the complex stiffness damper.

Fig. 10 shows the SDOF model for the target building, and Table 4 provides its specifications. Fig. 11 shows the time history waves of relative story displacement and damping force for an MR damper operated with complex stiffness control and the time history response analysis using the target complex stiffness damper when a 150% El Centro wave is input. As Fig. 11 shows, the proposed complex stiffness control can simulate the target performance.

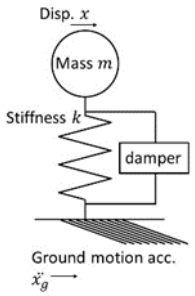

Fig. 10 – SDOF model for target building

Table 4 – Specifications of SDOF model

Mass	14,900 kg
Stiffness	38,500 N/m

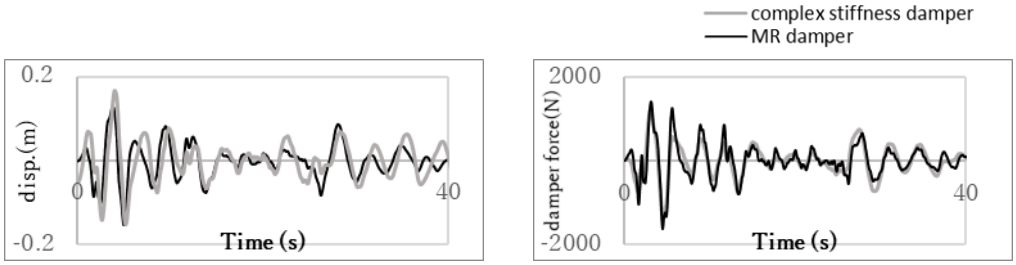

Fig. 11 – Time history waveforms of displacement (left) and damping force (right) for MR damper and target complex stiffness damper response to 150% El Centro wave

3.2 Shaking table test

An E-Defense shaking table test was conducted using the base-isolated testbed and an MR damper controlled by the strategy presented in subsection 3.1. The test parameters are shown in Table 5. Fig. 12 shows the time history waveforms of the relative story displacement for the isolation layer when the MR damper was operated with the complex stiffness control and controlled to simulate the viscous damping in response to El Centro, Takatori, and Sylmar waves. As Fig. 12 shows, there is little difference in the isolation layer drifts between the complex stiffness control and passive viscous damping; that is, both control strategies exhibit almost the same reduction of the displacement response. Fig. 13 shows the corresponding time history waveforms of absolute floor acceleration, and Fig. 14 shows those for the damping force. There is little difference in the floor accelerations between complex stiffness control and viscous damping, as seen in the isolation layer drifts. However, the damping force of complex stiffness control is less than that of viscous damping in response to all input earthquake waves, as shown in Fig. 14. Therefore, the proposed complex stiffness control can reduce the damping force in comparison with the viscous damping force. The complex stiffness control can originally reduce absolute floor acceleration in comparison with the viscous damping, because of the reduced damping force. It is considered that the absolute accelerations of complex stiffness control in the E-Defense test are not reduced because of the difference between the designed digital filter and the target filter, and a more appropriate design for the digital filter is desired.

Table 5 – Test parameters

Mass	14,900 kg	β	0.10
Stiffness	38,500 N/m	h	0.10
		ω_0	1.61

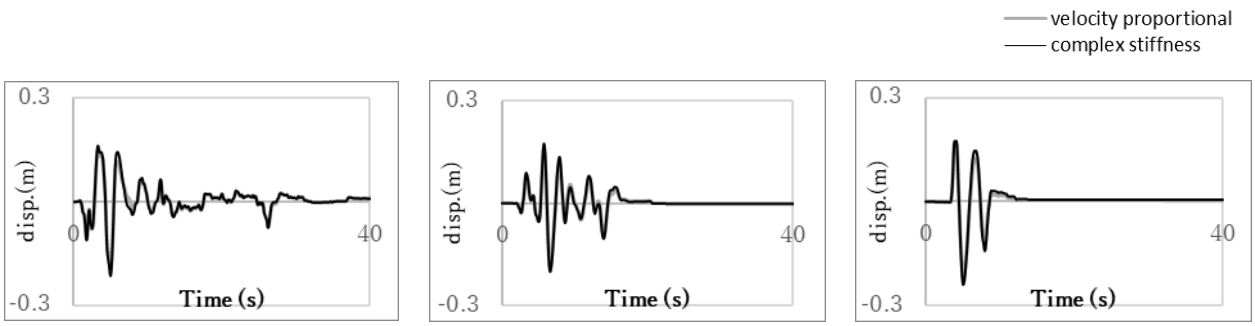

(a) El Centro (b) Takatori (c) Sylmar

Fig. 12 – Time history waveforms of isolation layer drift for complex stiffness damper and passive viscous damper, when El Centro, Takatori, and Sylmar waves are input

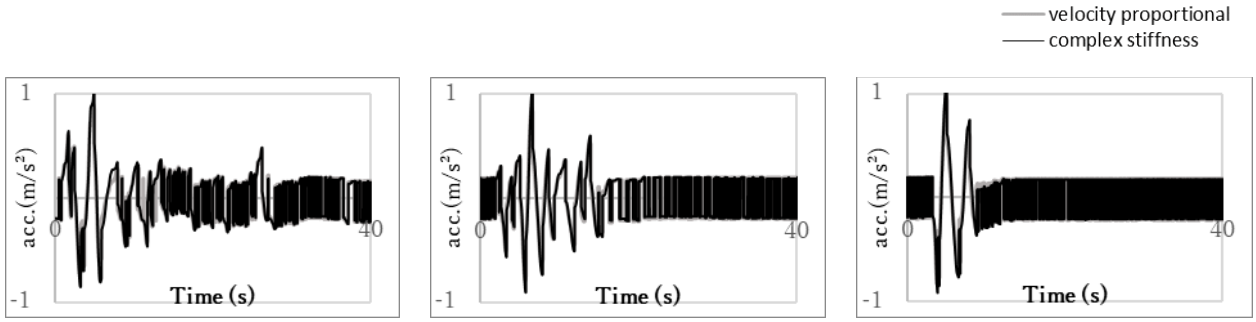

(a) El Centro (b) Takatori (c) Sylmar

Fig. 13 – Time history waveforms of absolute floor acceleration for complex stiffness damper and passive viscous damper when El Centro, Takatori, and Sylmar waves are input

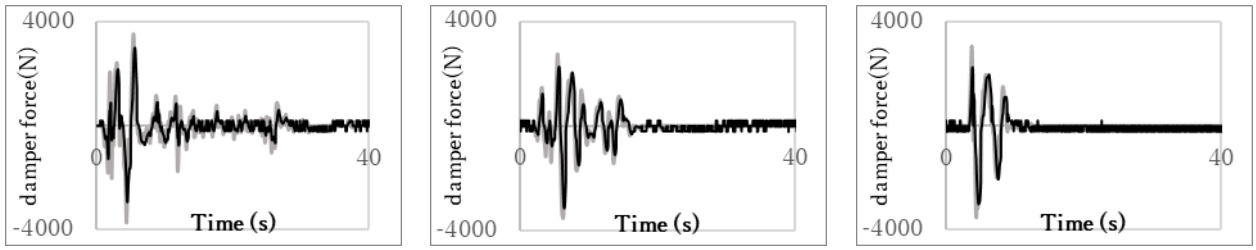

(a) El Centro (b) Takatori (c) Sylmar

Fig. 14 – Time history waveforms of damping force for complex stiffness damper and passive viscous damper when El Centro, Takatori, and Sylmar waves are input

4. Conclusions

With the purpose of reducing the seismic response of a base-isolated structure, two control strategies for an MR damper were proposed. Shaking table tests of a base-isolated specimen with an MR damper were conducted at E-Defense, and the proposed control methods were verified.

A control system that simulates a semi-active hydraulic damper, which switches the damping coefficient between two phases, was designed based on LQR control. To prevent chattering, a new control strategy was proposed. E-Defense and RTHS tests using an MR damper controlled by the proposed strategy were conducted. Our proposed control system performed almost the same as passive viscous damping for the drift of the isolation layer. Furthermore, it could restrain an increase in the absolute acceleration caused by a larger damping coefficient, as compared with the passive damper.

To simulate the complex stiffness damper using an MR damper, complex stiffness control was developed by designing a Butterworth filter and phase-delay-compensation filter. The behavior of the MR damper operated with the complex stiffness control agreed with the time response analysis results of the complex stiffness damper using transfer functions in the frequency domain. The results of E-Defense testing showed that the damping force of the complex stiffness damper was reduced in comparison with the force of the passive viscous damper. A more adequate design for the digital filters is desired to further reduce the response accelerations.

5. Acknowledgements

This work was supported by JSPS Grant No. R2904 in the Program for Fostering Globally Talented Researchers and the research unit of Multidisciplinary Integration for Resilience and Innovation (MIRAI) in Kobe University.

6. References

[1] Yang JN, Agrawal AK (2002): Semi-active hybrid control systems for nonlinear buildings against near-field earthquakes. *Engineering Structures*, **24** (3), 271–280.

[2] Sahasrabudhe S, Nagarajaiah S (2005): Semi-active control of sliding isolated bridges using MR dampers: an experimental and numerical study. *Earthquake Engineering and Structural Dynamics*, **34**(8), 965-983.

[3] Hiwatashi T, Fujitani H, Saito T (2008): Fundamental study on damping performance and control characteristics of semi-active damper. *Journal of Structural and Construction Engineering* (AIJ), **73**(626) 519-525 (in Japanese).

[4] Kumagai N, Nakamura S, Ikenaga M, Ikago K, Inoue N (2014): A Study on Implementation of Complex Stiffness Damper for Base Isolated Structure by Using an MR damper. *Summaries of Technical Papers of Annual Meeting Architectural Institute of Japan*, B-II 495-498 (in Japanese).

[5] Sato E, Kishida A, Kajiwara K, Fujitani H, Mukai Y, Ito M, Itahara K, Johnson E, Christenson R (2020): OUTLINE OF E-DEFENSE SHAKING TABLE TESTS FOR SEMI-ACTIVE CONTROL OF BASE-ISOLATION SYSTEM. Proceedings of 17th World Conference on Earthquake Engineering, Paper N° C002561.

